Journal of The Electrochemical Society, **153** (8) B330-B335 (2006)
0013-4651/2006/153(8)/B330/6/$20.00 © The Electrochemical Society

The Relationship Between Pit Chemistry and Pit Geometry Near the Critical Pitting Temperature

M. H. Moayed[a,z] and R. C. Newman[b]

[a]*Department of Materials Engineering, Faculty of Engineering, Ferdowsi University, Mashhad, Iran*
[b]*Department of Chemical Engineering and Applied Chemistry, University of Toronto, Toronto, Ontario, Canada M5S 3E5*

In pitting corrosion, the pit stability product is the product of anodic current density and depth, *ia*, which for an open hemispherical cavity would be proportional to the product of the cation diffusivity and some interfacial concentration of the dissolving cations, *DC*. Many authors believe that pit growth is diffusion-controlled, i.e., $C = C_s$ (solubility of the metal salt). Temporarily, prior to salt film precipitation, supersaturation is possible up to some maximum value: $C = C_{ss}$. Estimates of *ia* for real pits can be used to analyze their degree of occlusion, that is, by how much the effective value of pit radius ($a_{eff} = \alpha nFDC_s/i$, where α is a geometrical factor close to 0.5) differs from the geometrical pit radius calculated using Faraday's law (a). Small pits are found to be highly occluded, i.e., $a_{eff} \gg a$. For metastable pits formed in a high-alloy 904L stainless steel, the value of *ia* increases linearly with pit depth, and for a temperature 7° below the critical pitting temperature (CPT), approaches DC_s at the largest observed pit depth of ca. 10 μm, but very large metastable pits formed closer to the CPT have *ia* values that exceed even DC_{ss}. We show that this is consistent with the time-dependent development of a dish-shaped pit geometry, and that by suitable correction the stability products become consistent with diffusion-controlled pit growth.
 [DOI: 10.1149/1.2210670]

Manuscript submitted April 4, 2005; revised manuscript received April 12, 2006. Available electronically June 16, 2006.

Pitting corrosion of stainless steel in chloride solutions shows critical potentials or temperatures for stability. Below the critical pitting temperature (CPT), pitting vanishes at all potentials.[1-3] Above the CPT, pitting occurs above a critical potential, the pitting potential. The CPT transition is governed by some deterministic process, while the pitting potential is a distributed quantity.

Metastable pitting is usually defined as pitting that occurs below the pitting potential in tests conducted above the CPT.[4,5] Pits grow for a while but then repassivate, giving characteristic anodic current transients. However, another form of metastable pitting occurs over a wide range of potentials at temperatures below the CPT.[3] Such pits show different behavior from the usually studied pits that occur above the CPT but below the pitting potential. For example, the apparent nucleation frequency of metastable pits below the CPT shows a peak at intermediate potentials[3] that has been ascribed to a new role of the anodic salt film: not as a stabilizing factor for pit dissolution but as an intermediate in pit repassivation (as in the passivation of iron in sulfuric acid, which occurs under a ferrous sulfate salt film). According to this argument, pits survive longer at lower potentials because it takes longer to precipitate the salt film. The actual pit initiation frequency might be increasing or even decreasing with increasing potential, but with a given current resolution it appears that there are more transients at intermediate potentials. This represents a fundamentally different view from that of Pistorius and Burstein,[5] who believed that a salt film was present from the instant of pit nucleation.

The idea that the CPT is related to a change in the role of the salt film probably contains a great deal of truth, but in recent work[6-8] we have laid more emphasis on the nonuniformity of the dissolution rate within a pit. The observation of very large, open, metastable pits just below the CPT, yet with mostly electropolished interior surfaces, led to the suggestion that it is not the ability of the pit base to keep dissolving that is critical but the ability of the pit to undercut the surface, forming a lacy metal cover that hinders outward diffusion from the pit. Upon passivation near the pit rim, due to local dilution, the creation of a boundary between active and passive areas allows a very high current density to flow locally under ohmic control; undercutting can thus proceed at a very high rate to form a stable pit, but only if that extreme anodic current density does not exceed the critical current density for passivation in the local environment. At some temperatures, the pit base will be able to dissolve at its diffusion-controlled rate, but the necessary higher rate at the undercutting site will not be accessible; that temperature will be the CPT.

In order to track the conditions within a small pit while it is growing, we first compare its current–time behavior with that expected for an open, hemispherical cavity that is dissolving uniformly. We are able to do this because Pistorius and Burstein[5] obtained good agreement of current transients from most of their open pits with the following modified one-dimensional Fickian equation

$$D \cdot \Delta C = \left(\frac{2\pi}{3nF}\right) ia \qquad [1]$$

where a is the pit radius, i the uniform anodic current density in the pit, ΔC the concentration difference of dissolved cations between the pit base and the pit mouth, and D the cation diffusivity (assumed not to be a function of C, which is reasonable because all pits grow fairly near their saturation condition; Pistorius and Burstein believed they were always at that condition). For stainless steel, dissolving as Fe II, Ni II, and Cr III, and neglecting Mo, n is about 2.2.

The product *ia* is called the stability product. If all pits have a constant value of $D(\Delta C)$, corresponding to saturation on the pit surface and a negligible concentration gradient outside the pit, then the saturation concentration of metal salt, C_s, can be substituted for ΔC in the above equation. Then a measurement of *ia* for a naturally growing pit gives us information on the degree to which the pit is occluded by corrosion product, porous metal, or any other diffusion barrier, that is, transport within an occluded pit is governed by an effective radius, a_{eff}

$$a_{eff} = \frac{3nFDC_s}{2\pi i} \qquad [2]$$

Usually such barriers stabilize pitting. The stability product for an open, truly one-dimensional cavity growing in its diffusion-controlled state can be measured separately using the pencil electrode or artificial pit technique[6,7,9,10]

$$DC_s = \frac{i_L h}{nF} \qquad [3]$$

where i_L and h are the anodic limiting current density and the depth of the cylindrical pit, respectively.

Aside from the saturation concentration of metal salt, C_s, two other concentrations (or rather *DC* products - separation of D and C can only be achieved using transient techniques) can be measured using the steady-state pencil electrode technique: the maximum su-

[z] E-mail: mhmoayed@um.ac.ir

Table I. Compositions of the alloys used in this work.

Grade	Main alloying elements (wt %, balance Fe) Cr	Ni	Mo	Mn	N	Other
302[a]	17–19	7–11	-	<2	-	-
316[a]	17–20	10–12	2.0–3.5	<2	-	-
904L[b]	20.06	25.04	4.32	1.41	0.06	Cu

[a] Nominal composition supplied by Goodfellow Metals.
[b] Actual composition supplied by Avesta Sheffield.

persaturation concentration prior to salt precipitation, C_{ss}, and the critical concentration below which repassivation occurs, C^* (recognizing that these may depend on pit depth to some extent). Simplistically, the CPT is the temperature where $C^* = C_s$. This explains why the CPT, for alloys with consistent nucleation site geometries, is a relatively deterministic transition compared with the pitting potential and does not depend on chloride concentration in the bulk solution.[2,3,10] C^* is not discussed further in this paper.

We can use the pencil electrode technique to measure DC_s and DC_{ss} as a function of temperature using a generic stainless steel that is available as a thin wire and apply those values to the analysis of metastable pitting in a high-alloy material such as 904LSS. We first confirm, by comparing 302SS and 316SS, that alloyed Mo does not affect the limiting current density significantly.

Experimental

Experimental materials.— All materials used were austenitic stainless steels. Three grades of stainless steel were used, including 50 μm 302 and 316 SS wires, supplied by Goodfellow Metals, and the highly alloyed 904L stainless steel supplied by Avesta-Sheffield. The 302 and 316 SS were used for the artificial pit electrode experiments. The alloy compositions are given in Table I.

Artificial pit (pencil) electrodes.— For pencil electrode experiments, 50 μm wires of 302 and 316 SS were used. The electrodes were made by mounting the wires in epoxy resin in a U-shaped 6 mm glass tube so that one end of the wire could be abraded to expose a disk electrode. The other end of the wire was connected to shielded copper wire, which was inserted into another 6 mm glass tube. The electrode surface faced upward in all experiments. The working electrodes used in this work were wet polished to a 320 grit finish, using silicon carbide paper, and washed with deionized water prior to each experiment.

Plain electrodes.— Specimens from a 6 mm plate of 904L high-alloy stainless steel were cut with a surface area of 5 cm^2 for CPT measurements and 0.1 cm^2 for recording of metastable pit current transients. The specimen was welded to Nichrome wire for electrical connection. The connection wire was covered with a heat-shrinkable plastic tube to provide insulation from the external environment. Specimens were mounted in resin and allowed to set overnight in air. They were mechanically wet polished to a 3 μm diamond paste finish, degreased with ethanol, and dried with air. Then the junction between the resin and the metal was masked with a lacquer and dried with warm air. This method of preparation gave almost 80% of test specimens that avoided crevice corrosion. Discrimination between pitting and crevice corrosion is easy in experiments performed below the CPT, because there is no stable pitting and crevice corrosion is marked by a slow, steady current increase; when the latter occurred, the result was discarded.

Electrochemical procedures.— The electrochemical cell was a 250 mL beaker open to air. From 150 to 200 mL of solution were used for each experiment. Artificial pit and plain electrodes were simply dipped into the solution. A commercial Ag/AgCl reference electrode was used for all experiments. The auxiliary electrode was a bright platinum sheet, area ~2 cm^2, assembled on a glass tube. Temperature was controlled by a water bath.

An ACM potentiostat (ACM Instruments) was used to control the electrode potential. The potential was scanned using an ACM sweep generator (ACM Instruments) or 16-bit Miniscan (Thompson Electrochem, Ltd.). The current between working and auxiliary electrodes was measured either by a digital electrometer in series with the cell or across a resistor inserted into the circuit. The analog output of the electrometer or current output of the potentiostat was connected to an A/D card and the data were stored in a PC. Exploratory artificial pit experiments were done using a chart recorder to record the current.

Microscopy.— Scanning electron microscopes (AMRAY 1810 and ISI-DS130) with secondary electron detection and energy-dispersive X-ray facilities were used to examine the detailed features of as-pitted and ultrasonically cleaned specimens. Surface conductivity of the specimen was improved by carbon coating. Accelerating voltages up to 20 kV were used.

Pit mouth radii s were measured for a complete population of pits grown at 54°C using an optical microscope. The values of s were averaged around the perimeter. The estimated error in s is 5%. Pit depths h were measured for representative pits using a micrometer needle depth gauge to check that the values of $s/2h$ deduced from comparison of s with the anodic charge passed in a pitting event were valid; subsequently the latter method was relied upon for the data analysis.

Potentiostatic measurement of critical pitting temperature.— This procedure was described elsewhere.[3,8] The CPT of the 904L alloy for this surface finish was 56°C.

Potentiostatic measurement of metastable pit current transients.— The metastable pit current transient measurements were carried out at 750 mV (vs Ag/AgCl) in 1 M NaCl (open to air) at several temperatures. The main aim of these experiments was to calculate the anodic current density as a function of pit radius for individual metastable pit transients, so small working electrodes of ~0.1 cm^2 were used to reduce overlap of transients. The working electrode was held at its rest potential for 5 min, then polarized with a scan rate of 10 mV/s to 750 mV vs Ag/AgCl (this reduced the incidence of crevice corrosion compared with stepping the potential). The current transients were recorded from 5 s after application of the potential. A 60 Hz data acquisition rate was used; for the briefest and steepest transients analyzed, this gave a resolution of better than 1% of the peak current.

Measurement of critical pit chemistry parameters using pencil electrodes.— The artificial pit electrode measurements were carried out in a 250 mL beaker of 1 M NaCl solution with a three-electrode system at several constant temperatures. After initial stabilization of the temperature with the electrode at its open-circuit potential, a potential of 750 mV vs Ag/AgCl was applied. Formation and coalescence of salt-covered pits led to a steady-state, diffusion-controlled condition, giving a value for DC_s. After the required amount of diffusion-controlled growth, the potential was stepped to 300 or 400 mV prior to backward scanning the potential to measure DC^* (these data are not discussed here; values of the ratio C^*/C_s varied from 0.4 to 0.8). In order to measure the DC value corresponding to the maximum supersaturation concentration of pit solution, C_{ss}, the direction of scanning was reversed just after entering the activation/IR-drop-controlled regime on the backscan. This allowed dissolution of the salt film so that the conditions for its reprecipitation on the forward scan could be measured.

Results and Discussion

Pit chemistry measurements using artificial pit electrodes.— Demonstration of lack of sensitivity to Mo content.— Figure 1 shows plots of i^2 vs t^{-1} for pencil electrodes of 302SS and 316SS, confirm-

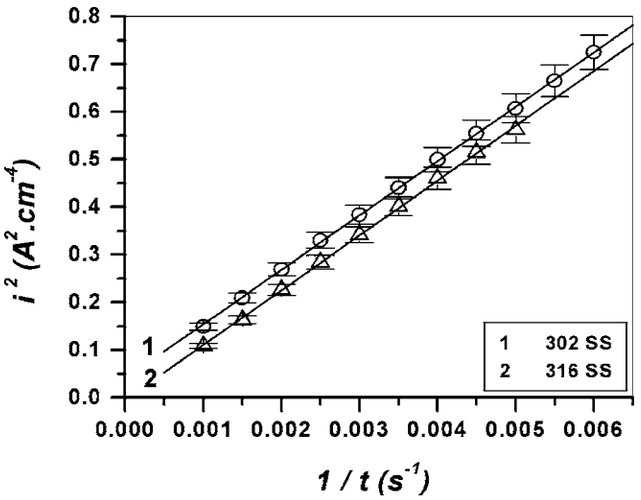

Figure 1. Plots of i^2 vs $1/t$ obtained from the current density–time curves using pencil electrodes of 50 μm 302 and 316 SS wire in 1 M NaCl solution at 750 mV (vs Ag/AgCl) at 40°C.

ing that the negligible effect of Mo on diffusion-controlled dissolution, shown previously at room temperature,[7] is valid for higher temperatures such as 40°C. Part of the difference between the two lines in this plot is due to differences in the initial coalescence of pits before uniform dissolution was established; also, as noted by Laycock,[9] the diffusion-controlled current is noisy at high potentials due to local passivation-reactivation events, and if the frequency of these events differs between alloys, this could slightly bias the mean current in one direction or the other.

Measurement of DC_s and DC_{ss} at different temperatures using 302SS.— The principle of this measurement is shown in Fig. 2. DC_s is determined from the diffusion-controlled current density. Point *a* is the transition potential between active and diffusion-controlled dissolution and point *c* corresponds to the maximum supersaturation of the pit solution and gives us DC_{ss}. The fact that the pit grows during such a measurement has to be taken into account (i.e., the fact that current density *a* is higher than current density *d*, the best comparison made using points *c* and *d*).

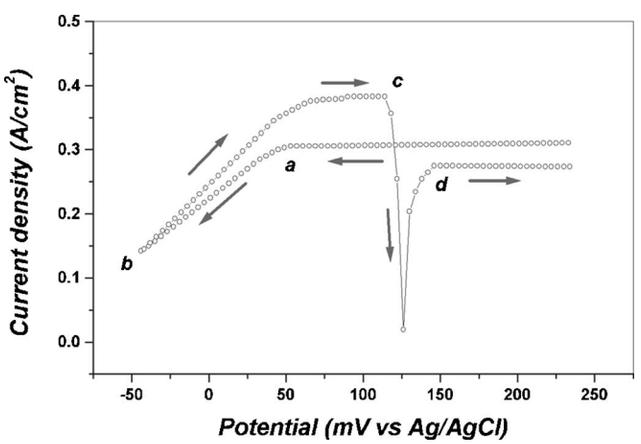

Figure 2. Cyclic behavior of a pencil electrode (artificial pit) of 302 SS in 1 M NaCl solution at 40°C (potential scan rate 4 mV/s). After growing the pit at 240 mV, the potential is scanned downward: Diffusion-controlled dissolution gives way to ohmically controlled dissolution at point *a*. After scan reversal at point *b* the solution supersaturates and a thick salt film precipitates at point *c* to relieve the supersaturation, diffusion control resumes when this has mostly dissolved away.

Table II. Average values of DC_s and DC_{ss} at different temperatures, determined using pencil electrodes of 50 μm 302 SS in 1 M NaCl solution.

Temperature (°C)	DC_s (mol/cm s)	DC_{ss} (mol/cm s)
40	5.81×10^{-8}	7.26×10^{-8}
45	6.52×10^{-8}	8.15×10^{-8}
49	7.18×10^{-8}	8.98×10^{-8}
54	7.96×10^{-8}	9.95×10^{-8}
59	8.41×10^{-8}	10.51×10^{-8}
63	9.23×10^{-8}	11.53×10^{-8}

Table II shows the values of DC_s and DC_{ss} obtained under the criterion that the values did not vary by more than 5% with changes in pit depth between 100 and 150 μm or changes in potential scan rate around 4 mV/s. Values of DC^*, not shown here, increased more slowly with temperature than DC_s; thus, the ratio of C^*/C_s decreases with increasing temperature, as expected. The DC_s and DC_{ss} values were calculated for each temperature using Eq. 3, as shown in Table III.

Current transients of metastable pits.— Metastable pitting current transients were studied using 904L austenitic stainless steel with a 3 μm diamond-paste finish at 750 mV (vs Ag/AgCl) in 1 M NaCl solution at two temperatures below the alloy CPT. Figures 3 and 4 display the characteristic shape of these transients at 49 and 54°C.

By assuming a hemispherical geometry, a density of 8.00 g/cm^3, and an average of 2.2 electrons transferred per atom dissolved, the pit current density and stability product could be calculated as a function of time. For very large transients recorded at 54°C, corresponding to large metastable pits with polished internal surfaces (Fig. 4; Ref. 8), the current density appeared to be nearly constant (Fig. 5) and the stability product increased steeply with time (Fig. 6). The apparently constant current density should not be interpreted as "activation control" of pit growth but is due to a change in pit geometry with time, so that the ohmic or diffusionally controlled current density departs from the $t^{-0.5}$ law seen for a one-dimensional cavity. These data were obtained assuming a linear variation of the background passive current during the life of each transient; for large transients like the one in Fig. 5, the result was indistinguishable from that calculated with a constant background. For smaller transients the possible error due to the background subtraction had a small effect on the stability product calculated at the point of repassivation, which is the main point of the paper. The error is about the size of the symbols in our figures.

There was some minor oscillation in the current–time curves which was amplified when calculating current densities or stability

Table III. Values of pit stability product (*ia*), corresponding to saturation and supersaturation conditions of the pit, obtained using 50 μm pencil electrodes of 302 SS in 1 M NaCl at different temperatures.

Temperature (°C)	Corresponding stability product *ia* (A/cm) to achieve C_S	Corresponding stability product *ia* (A/cm) to achieve C_{SS}
40	5.86×10^{-3}	7.32×10^{-3}
45	6.61×10^{-3}	8.27×10^{-3}
49	7.21×10^{-3}	9.01×10^{-3}
54	7.94×10^{-3}	9.93×10^{-3}
59	8.48×10^{-3}	10.65×10^{-3}
63	9.09×10^{-3}	11.37×10^{-3}

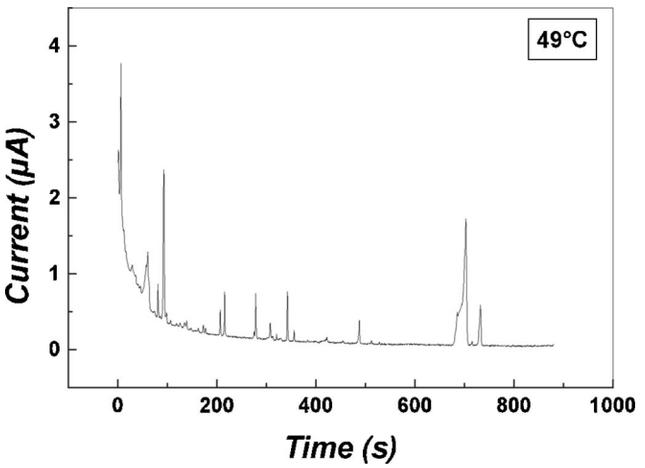

Figure 3. Metastable pitting events observed 7° below the CPT for type 904L stainless steel held at 750 mV (vs Ag/AgCl) in a solution of 1 M NaCl at 49°C; CPT ≈ 56°C.

products at short times after pit initiation. This was not due to insufficient rate of data acquisition, and none of the interpretation relied on the behavior at such short times.

Values of pit stability product lower than those calculated from the artificial pit data are due to occlusion of the pit, so that the effective pit depth a_{eff} is greater than its geometrical one. This was typical for the smaller transients recorded at 49°C (Fig. 7) and gives valuable information on the pit geometry. For pits to grow even temporarily at these temperatures, they must be very occluded, and repassivation occurs when the stability product approaches that for an open pit. For the larger subpopulation of transients at 54°C shown in Fig. 4, the pit stability product apparently increases above the maximum value determined for the artificial pits, even assuming supersaturation of the pit solution (Fig. 8).

Figures 7 and 8 both give good linear correlations between the stability product and the pit depth. This is not understood quantitatively at present but could be rationalized by assuming that the pits initially undercut the surface, leaving a small exit hole (as observed many times by SEM), but then the hole in the pit cover grows as fast or faster than the pit depth. This would naturally lead to a cavity that

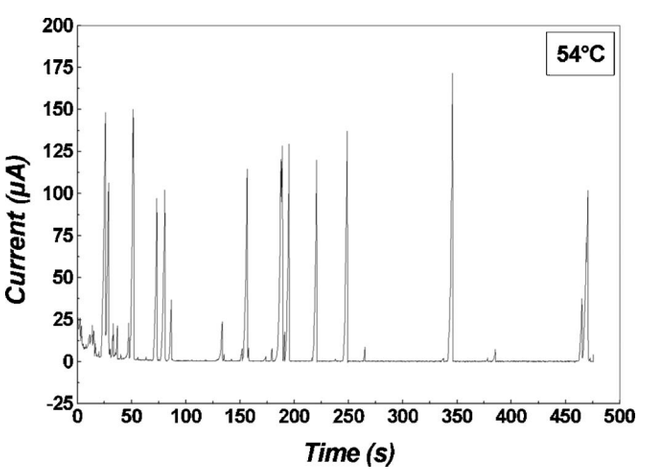

Figure 4. Very large metastable pitting events observed just below the CPT for 904L stainless steel held at 750 mV (vs Ag/AgCl) in a solution of 1 M NaCl at 54°C; CPT ≈ 56°C.

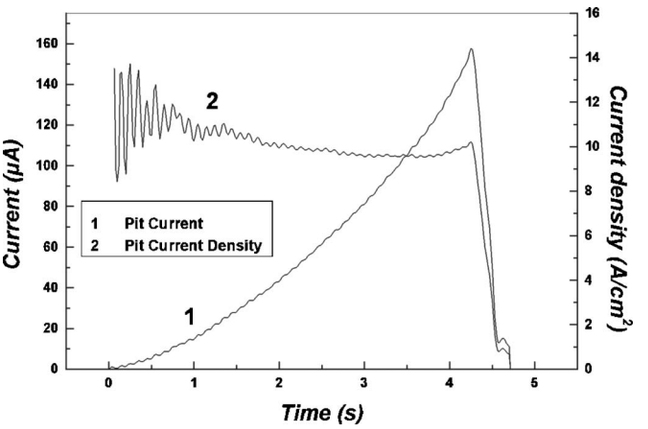

Figure 5. Metastable pit current and current density plots (assuming hemispherical pit growth) for 904L SS at 54°C.

with time becomes more and more equivalent to a fully open one. We do not have an analytical model for this process; numerical modeling is in progress.

The anomalous values of stability product at 54°C shown in Fig. 8 could be due to development of a dish-shaped pit geometry for the larger pits. This was confirmed for two representative pits using the micrometer depth gauge; for the pit shown in Fig. 9, $s/2h$ was 1.37. This validated the simpler method of measuring the widths (s) of a large number of the large repassivated pits formed at 54°C and calculating the discrepancy between $s/2$ and the hemisphere radii equivalent to the anodic charges recorded for the associated transients. The smaller pits had to be discarded due to varying geometry, interference from inclusion remnants, etc., leaving the 14 largest pits for the correlation. By ordering from largest to smallest, pits could be associated with particular transients, leading to the correlation shown in Fig. 10. This gives information on the distribution of pit geometries just before repassivation; death of these large metastable events is due to their inability to undercut the surface to generate a lacy metal cover, leading inevitably to widening and eventual repassivation.[8] We note that the pits of intermediate size have even larger departures from hemisphericity than the largest ones. This seems a real result and perhaps indicates that a few pits grew under microscopic surface laps or other defects, then repassivated after bursting through to the surface. Current transients of individual pits did not show a time evolution consistent with Fig. 10.

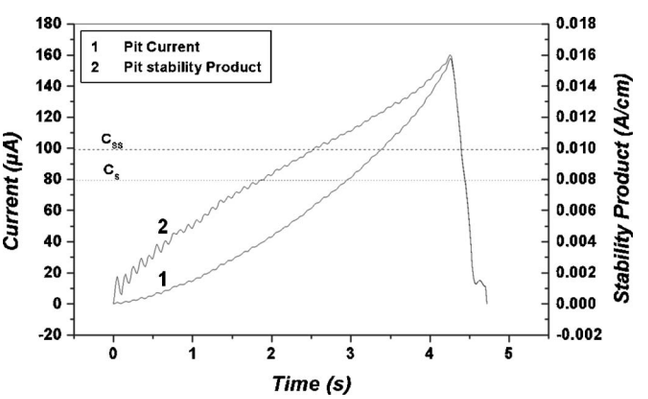

Figure 6. Metastable pit current and stability product plots (assuming hemispherical growth) for 904L SS at 54°C (same pit as Fig. 5). Stability products associated with C_s and C_{ss} at 54°C are illustrated by two horizontal lines.

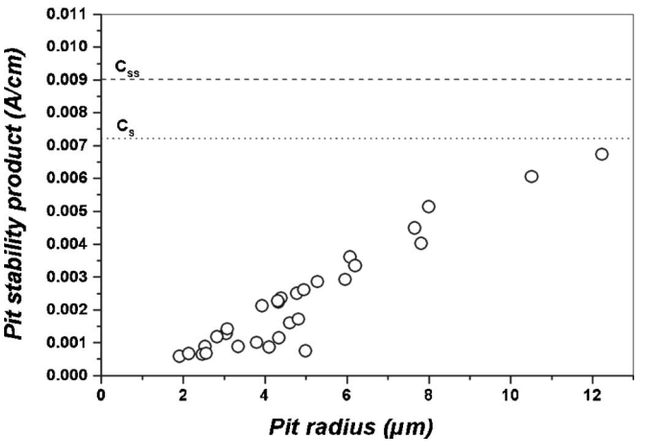

Figure 7. Distribution of metastable pit stability product (*ia*) at repassivation as a function of pit radius (assuming hemispherical pit growth) for 904L SS at 49°C. Stability products associated with C_s and C_{ss} at 49°C are illustrated by two horizontal lines.

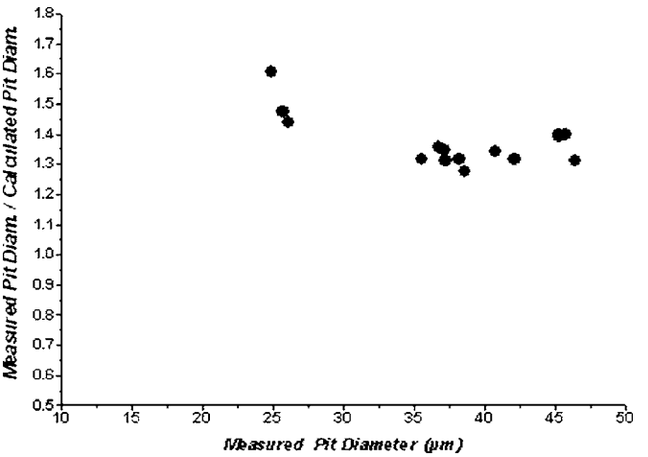

Figure 9. Comparison between the measured mouth diameter of metastable pits and the diameter calculated from the anodic charge on the assumption that the pits are hemispherical, for 904L SS at 54°C.

Current density and pit stability product of a dish-shaped pit.— The current density of a dish-shaped pit is different from a hemispherical pit with the same current. Consider a sphere segment geometry with $s/2h = 1.37$, where s and h are the width of the mouth and the depth of the segment.

The volume (V) and surface area (A) of a sphere segment can be calculated from s and h as follows

$$V = \frac{\pi h}{6} \times \left(\frac{3}{4}s^2 + h^2\right) \quad [4]$$

$$A = \frac{2\pi}{5}(s^2 + h^2) \quad [5]$$

Because we do not have comprehensive geometry data for the smaller pits, we have to make some assumptions about how this geometry evolves. Despite the shape of the correlation in Fig. 10, we know that covered pits in the range of a few micrometers are more nearly hemispherical than those of 20–50 μm shown in Fig. 10. We therefore assume that the evolution in pit shape from hemispherical to dish-shaped occurs gradually from the start of pit growth. There is an underlying assumption that there is always a small projection of the passive film at the pit rim, which prevents instant passivation there. Such an assumption is well grounded in the literature;[4] we know that Cr-rich passive films on stainless steels cannot dissolve at rates equivalent to the A/cm^2 at which these pits are growing.

Consider the metastable pit current transient recorded at 54°C shown in Fig. 5 and 6. This is a typical transient of a dish-shaped pit. In order to estimate the current density of that transient as a function of time, we assume that $s/2h$ evolves gradually from 1.00 and reaches 1.37 at the moment of repassivation. Considering values of $h = K_1 a$ and $s/2 = K_2 a$ for the dish geometry, in which K_1 and K_2 are the dimension factors and a is the radius of the equivalent hemisphere, Table IV gives the values of K_1 and K_2 for the different stages of pit lifetime of the transient illustrated in Fig. 5 and 6, assuming that K_1 and K_2 change linearly with time of pit growth.

At repassivation ($t = 4.25$ s) the ratio $s/2h$ is set to 1.37 as required by the experimental data. Then the values of h and $s/2$ were calculated from the pit radius–time (a–t) curve of the equivalent pit with a hemispherical geometry. Figure 11 illustrates the variations in a,h, and $s/2$ as a function of pit growth time.

Variation of the current density with time at the bottom of a dish (depth h) can be calculated as follows

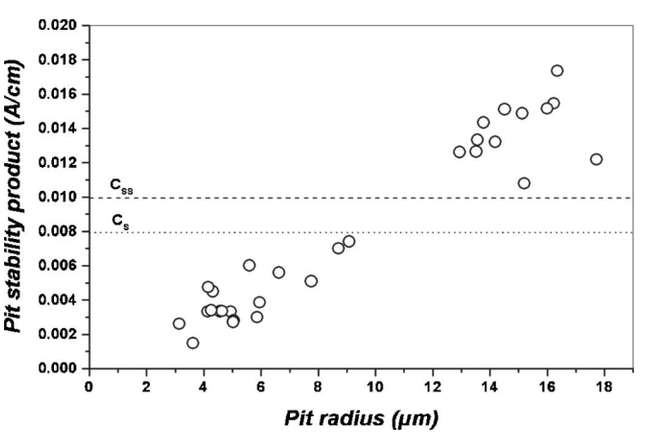

Figure 8. Distribution of metastable pit stability product (*ia*) at repassivation as a function of pit radius (assuming hemispherical pit growth) for 904L SS at 54°C. Stability products associated with C_s and C_{ss} at 54°C are illustrated by two horizontal lines.

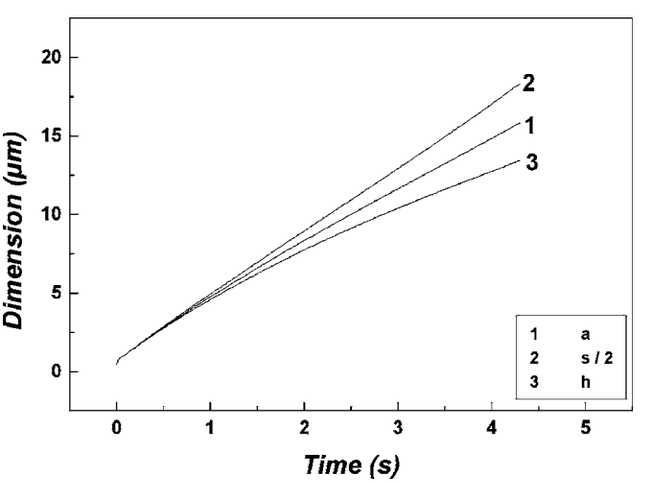

Figure 10. Variation of radius of equivalent hemispherical pit (a), sphere segment depth (h), and sphere segment mouth radius ($s/2$) as a function of pit lifetime for the metastable pitting current transient illustrated in Fig. 5 and 6, assuming that shape factors vary linearly during pit growth.

Table IV. Shape factors K_1 and K_2 for a pit developing from a hemisphere into a dish shape.

Time (s)	K_1	K_2
0	1.000	1.000
1	0.964	1.037
2	0.928	1.074
3	0.893	1.110
4	0.858	1.147
4.25 (repassivation)	0.850	1.156

$$i = \frac{nF\rho}{M_w} \cdot \frac{dh}{dt} \quad [6]$$

Figure 11 shows the comparison of the pit current density for hemispherical and dish-shaped geometries with the same volume. The calculated current density of the dish-shaped pit follows a decreasing trend of current density with time, which is the normal behavior for a process under diffusion control, except in the moments before repassivation. The current density vs time curve does not approach $i \sim t^{-0.5}$, because early in pit growth the pit is more closed than assumed but is opening up with time; this flattens the early part of the decay in current density. Recalculation of the stability product (ih) for a dish-shaped pit shows a value lower than the corresponding value for a hemispherical pit. Figure 12a illustrates the plots of stability product for dish and hemisphere pits for the metastable pit current transient illustrated in Fig. 5 and 6. It is evident that the maximum value of this recalculated (true) stability product for a dish-shaped pit is now more realistic when it is compared with the stability products associated with C_{ss} and C_s. The result is consistent with the view that as the pit approaches repassivation, it becomes a nearly open cavity with a salt film on (most of) its surface. Figure 12b shows the result for another pit.

Numerical simulations should be performed to clarify the validity of this approximate analytical approach.

Conclusions

1. Pit stability products as a function of temperature have been determined for a simple stainless steel using artificial pit electrodes and then used to understand the behavior of metastable pitting in a high-alloy steel at high potentials below the CPT.

2. Several degrees below the CPT, stability products are initially low, indicating occlusion of the pit, then rise to values consistent with an open hemispherical pit just before repassivation.

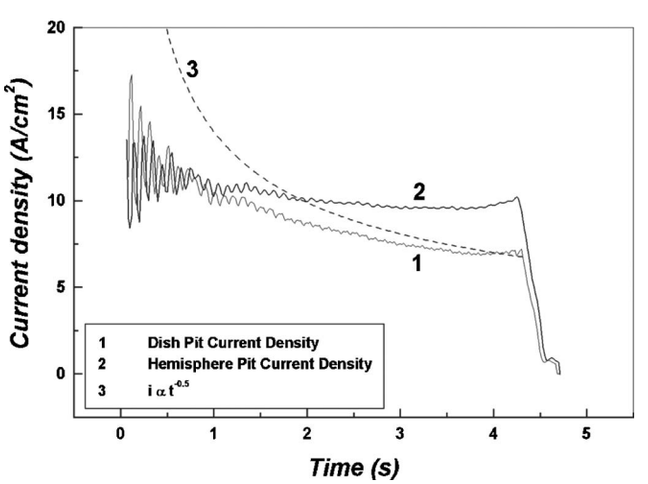

Figure 11. Current density within a metastable pit on 904L SS at 54°C with the assumption of hemispherical and dish-shaped geometries.

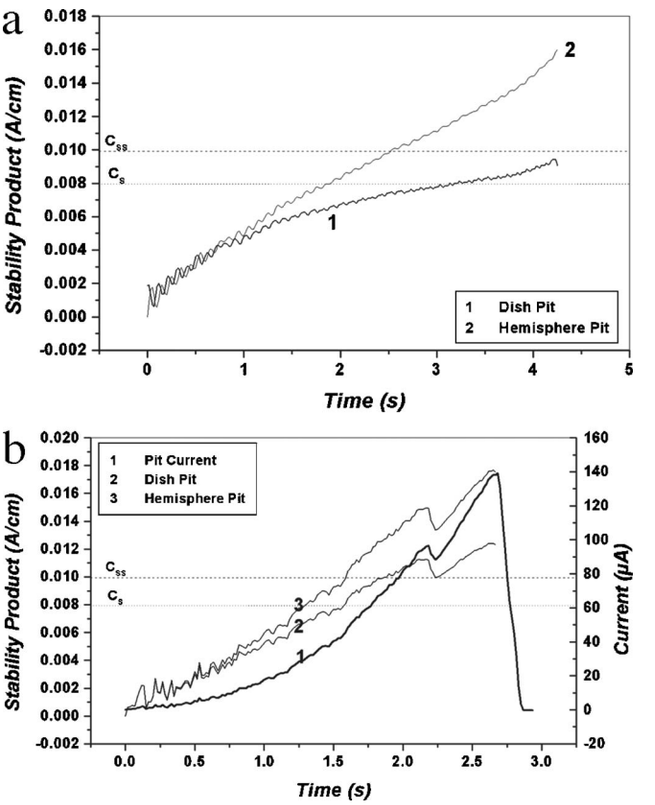

Figure 12. (a) Plot of pit stability product for the metastable pit transient of Fig. 11 (904L SS at 54°C) with the assumption of hemispherical and dish-shaped geometries. Dashed and dotted horizontal lines indicate the stability products associated with C_{ss} and C_s at 54°C. (b) Data for another pit showing a similar adjusted stability product value but a more complex repassivation sequence.

3. Very near the CPT, where very large metastable pit transients occur, the stability product apparently rises to an impossibly high value, but this is due to development of a dish-shaped geometry.

4. When suitable correction is made for the dish-shaped geometry, the later stages of the pit growth kinetics become more consistent with anodic diffusion control, and the stability product does not rise higher than values that are consistent with the artificial pit experiments.

Acknowledgments

The first author wishes to thank the Iran Ferdowsi University of Mashhad for their financial support. We also thank Avesta Polarit for supplying the 904L stainless steel.

Ferdowski University of Mashhad assisted in meeting the publication costs of this article.

References

1. R. Qvarfort, *Corros. Sci.*, **29**, 987 (1989).
2. V. M. Salinas Bravo and R. C. Newman, *Corros. Sci.*, **36**, 167 (1994).
3. N. J. Laycock, M. H. Moayed, and R. C. Newman, *J. Electrochem. Soc.*, **145**, 2622 (1998).
4. L. Stockert, F. Hunkeler, and H. Boehni, *Corrosion (Houston)*, **41**, 676 (1985).
5. P. C. Pistorius and G. T. Burstein, *Philos. Trans. R. Soc. London*, **341**, 531 (1992).
6. P. Ernst and R. C. Newman, *Corros. Sci.*, **44**, 927 (2002).
7. P. Ernst and R. C. Newman, *Corros. Sci.*, **44**, 943 (2002).
8. M. H. Moayed and R. C. Newman, *Corros. Sci.*, **48**, 1004 (2006).
9. N. J. Laycock and R. C. Newman, *Corros. Sci.*, **39**, 1771 (1997).
10. R. C. Newman, *Corrosion (Houston)*, **57**, 1030 (2001).